Journal of The Electrochemical Society, **165** (2) E81-E88 (2018)
0013-4651/2018/165(2)/E81/8/$37.00 © The Electrochemical Society

A CFD Study with Analytical and Experimental Validation of Laminar and Turbulent Mass-Transfer in Electrochemical Reactors

A. N. Colli [z] **and J. M. Bisang**

Universidad Nacional del Litoral, CONICET, Programa de Electroquímica Aplicada e Ingeniería Electroquímica (PRELINE), Facultad de Ingeniería Química, S3000AOM Santa Fe, Argentina

This work presents numerical simulations, with validation considering analytical expressions and experimental results, of mass-transfer in electrochemical reactors under laminar and turbulent flows in ducts of rectangular and tubular shape. Sudden expansion at the reactor inlet and segmented electrodes are also analyzed. Computational fluid dynamics (CFD) simulations were performed solving the laminar or RANS equations with the Shear Stress Transport (SST) k-ω turbulence model using the open source code OpenFOAM in steady-state. For mass-transfer simulations, the averaged diffusion-convection equation was implemented and solved. A good agreement between mass-transfer simulations with experimental data and analytical results were attained for both laminar and turbulent flow. Discussions about the segmented electrode technique in order to obtain local mass-transfer data in laminar and turbulent flow are also performed.
 [DOI: 10.1149/2.0971802jes]

Manuscript submitted January 2, 2018; revised manuscript received January 12, 2018. Published January 27, 2018.

Knowledge of mass-transfer is required for an efficient design of different equipment in many industrial processes. Electrochemical reactors are frequently used in the industry to carry out diffusion controlled electrochemical processes. One of the critical factors in operation of such reactors is the local mass-transfer profile,[1] which is mainly determined by the electrolyte flow inside the reactor.[2]

Mathematically speaking fully developed laminar flow, and in some extent turbulent flow, with both developed and developing concentration boundary layers are easy to describe.[1] The cases with no or insufficient entrance lengths, having developing hydrodynamic and/or concentration boundary layers, are more difficult to analyze from an analytical point of view.[3] The recommended design procedures for these reactors are based either on empirical analysis of experimental data or simple extrapolations of those for fully developed flow situations. Both strategies have the drawback that they have been obtained in idealized conditions and cannot be used in a new geometry.

Due to both the hydrodynamic and the mass-transfer behavior are extensively documented for simple geometries (circular duct, annulus or parallel-plate), which becomes very suitable test case to corroborate the laminar-turbulent flow and mass-transfer conditions by means of numerical solvers. The empirical correlations of mass-transfer results show a high disparity between the relationships obtained by several authors in different geometries. For example, there are correlations that give higher mass-transfer coefficients in circular ducts[4–6] than in parallel plate reactors[7–9] or even annular reactors,[10] contradicting the tendency of analytical results from laminar flow. To overcome this controversial situation, and taking into account the analogy between friction factors and mass-transfer, correlations must involve geometric parameters characterizing the reactor configuration,[11] as was done by Jones[12] and Jones and Leung,[13] who proposed a modified Re number to consider the effect of the geometry on the friction factors in turbulent flow. Likewise, discrepancies in local mass-transfer studies seem to be due to the experimental method of measurement. The segmented electrode technique is usually applied, in which small cathodes are embedded in a large active cathode in order to determine local values of mass-transfer. The segments can produce small flow disturbances increasing the mass-transfer coefficient.[14] Thus, the implementation of a computational model is needed in order to predict and evaluate the above aspects.

This paper presents a numerical analysis, validated experimentally and by comparison with analytical expressions, about the mass-transfer behavior in laminar and turbulent fluid flow for parallel-plate and cylindrical reactors. A discussion about the segmented electrode technique, frequently used in order to obtain local mass-transfer coefficients, is also performed.

[z]E-mail: ancolli@gmail.com

Mathematical Modeling

The mass-transfer distribution along the reactor length can be expressed in terms of the local Sherwood number defined as

$$\mathrm{Sh}_y = \frac{d_h}{D} k_{m,y} = \frac{d_h}{c_b} \nabla c|_{\text{electrode surface}} \quad [1]$$

and the global value is given by

$$\mathrm{Sh} = \frac{1}{L} \int_0^L \mathrm{Sh}_y \mathrm{d}y \quad [2]$$

The calculation of the concentration gradient at the surface of the working electrode requires solving the steady-state time-averaged convection-diffusion equation including the turbulence diffusivity, D_T, according to

$$\boldsymbol{u} \cdot \nabla c = \nabla \cdot [(D + D_T) \nabla c] \quad [3]$$

with the simultaneous solution of the incompressible continuity equation

$$\nabla \cdot \boldsymbol{u} = 0 \quad [4]$$

and the Navier-Stokes equations for a steady-state, incompressible and Newtonian fluid without external forces

$$\boldsymbol{u} \cdot \nabla \boldsymbol{u} = -\nabla p + \nabla \cdot \left\{ (\nu + \nu_T) \left[\nabla \boldsymbol{u} + (\nabla \boldsymbol{u})^T \right] \right\} \quad [5]$$

In laminar flow calculations c represents the local concentration, $\boldsymbol{u}$ the local flow velocity and p the density normalized pressure. Likewise, D_T and the turbulent viscosity, ν_T, are zero. Under turbulent flow conditions Eqs. 4 and 5 characterize the Reynolds-averaged Navier–Stokes (RANS) equations where c, $\boldsymbol{u}$ and p are the time-averaged variables. In order to solve the proposed turbulent problem, two-equation eddy-viscosity models[15] are usually used as this procedure combines accuracy and computational speed improvements. Frequently, in most of the previous work,[16,17] the applied turbulence models are based on the ε-equation and a transport equation for the dissipation of the turbulent kinetic energy k. For the wall boundary condition there is the choice between wall functions or integration to the surface using a low turbulent Reynolds number (low-Re) formulation. Models based on the ε-equation with wall functions over-predict the turbulence length scale under flows with adverse pressure gradients, which in turn results in high wall shear stress and high mass-or heat-transfer rates.[18] To overcome this problem, the Shear Stress Transport (SST) k-ω turbulence model[19] was chosen due to its superiority over the rest.[20] The model combines the k-ω and the k-ε turbulence models such that the former is used in the inner region of the boundary layer and switches to the later in the free shear flow. The use of a k-ω formulation in

the inner parts of the boundary layer makes the model directly usable all the way down to the wall through the viscous sub-layer, hence the SST k-ω model can be used as a low-Re turbulence model without any extra damping functions.

In the proposed model, the turbulent kinematic viscosity is given by[21]

$$\nu_T = \frac{a_1 k}{\max(a_1\omega,\ SF_2)} \quad [6]$$

where a_1 is a constant, F_2 is a function given by Eq. 13, S is the invariant measure of the strain rate given by Eq. 14. The turbulence kinetic energy, k, and the turbulence frequency, ω, or specific dissipation rate (rate at which turbulence kinetic energy is converted into internal thermal energy per unit volume and time), which are defined by the following differential equations

$$\nabla\cdot(\boldsymbol{u}k) = \nabla\cdot[(\nu+\sigma_k\nu_T)\nabla k] + P_k - \beta^* k\omega \quad [7]$$

$$\nabla\cdot(\boldsymbol{u}\omega) = \nabla\cdot[(\nu+\sigma_\omega\nu_T)\nabla\omega] + \frac{\alpha}{\nu_T}P_k - \beta\,\omega^2 + 2(1-F_1)\frac{\sigma_{\omega 2}}{\omega}\nabla k\cdot\nabla\omega \quad [8]$$

where σ_k, σ_ω, β^*, α, β are closure coefficients. P_k is the turbulence kinetic energy production given by

$$P_k = \min\left(\nu_T\nabla\boldsymbol{u} : \left[\nabla\boldsymbol{u} + (\nabla\boldsymbol{u})^T\right],\ c_1\beta^* k\omega\right) \quad [9]$$

Each of the constants, under the general symbol ct, is a blend of an inner (1) and outer (2) constant, combined via

$$ct = ct_1 F_1 + ct_2(1-F_1) \quad [10]$$

The following auxiliary relationships are necessary for the calculations

$$F_1 = \tanh\left\{\left[\min\left(\max\left(\frac{\sqrt{k}}{\beta^*\omega d_p},\ \frac{500\nu}{{d_p}^2\omega}\right),\ \frac{4\sigma_{\omega 2}k}{CD_{k\omega}{d_p}^2}\right)\right]^4\right\} \quad [11]$$

being d_p the distance perpendicular to the wall

$$CD_{k\omega} = \max\left(\frac{2\sigma_{\omega 2}}{\omega}\nabla k\cdot\nabla\omega,\ 10^{-10}\right) \quad [12]$$

$$F_2 = \tanh\left\{\left[\max\left(\frac{2\sqrt{k}}{\beta^*\omega d_p},\ \frac{500\nu}{{d_p}^2\omega}\right)\right]^2\right\} \quad [13]$$

$$S = \frac{\sqrt{2}}{2}\sqrt{\left(\nabla\boldsymbol{u} + (\nabla\boldsymbol{u})^T\right) : \left(\nabla\boldsymbol{u} + (\nabla\boldsymbol{u})^T\right)} \quad [14]$$

It should be point out that F_1 and F_2 are blending functions which are equal to zero away from the surface (k-ε model), and switches over to one inside the boundary layer (k-ω model).

The turbulent diffusivity was evaluated from the turbulent Schmidt number, Sc_T, defined as

$$Sc_T = \frac{\nu_T}{D_T} \quad [15]$$

Table I. Closure coefficients.

Coefficients	value
σ_{k1}	0.85
σ_{k2}	1.0
$\sigma_{\omega 1}$	0.5
$\sigma_{\omega 2}$	0.856
β_1	0.075
β_2	0.0828
β^*	0.09
α_1	5/9
α_2	0.44
a_1	0.31
c_1	10.0
Sc_T	0.5

Several ways were proposed to determine Sc_T.[22,23] In this contribution, based on the Reynolds analogy, it is used a constant for the turbulent Schmidt number. This parameter has been obtained from tracer experiments, field work and mass- or heat-transfer experimental values and usually ranges between 0.2 and 1.7[24–26] with some anomalous values reported as high as 4.5.[23] Table I summarizes the constants adopted for the mathematical calculations.

The OpenFOAM[27] free software was used to compute the velocity and concentration fields. The velocity profiles inside the reactor were calculated with the SIMPLEC algorithm[28,29] by means of the simpleFoam routine in steady-state. The field of concentration was obtained with the use of two own routines[30] called concentrationFoam and turbulentConcentrationFoam based on the default scalarTransportFoam routine by using the velocity and ν_T profiles previously obtained. The boundary conditions and initial guess fields used in the calculations are summarized in Table II. The absolute tolerances for calculating the velocity, k, ω, pressure and concentration profiles and the relaxation factor are given in Table III. Rotational symmetry was used for the tubular configuration and an infinite aspect ratio was assumed for the parallel plate case what allows to solve a 3D problem as 2D, reducing computational cost. The computational region was divided into a structured mesh 300–2500 per 100–150 cells in y-z directions, respectively. A non-uniform mesh grading was used for the mesh size in the y and z direction, which was gradually varied according to different geometric progressions that allows having grid points inside the viscous sublayer. For those cases where fully developed laminar flow was solved, an analytical velocity profile was imposed at the inlet.[11,31] In the case of turbulent flow there was used an entry length that allows to have fully developed turbulent flow conditions when the fluid reaches the electrode.

Results and Discussion

Developed laminar flow in parallel-plate and cylindrical electrochemical reactors.—Assuming that the hydrodynamics is developed, the local and global mass-transfer behavior is given by the following

Table II. Boundary conditions.

Field	Inlet	Outlet	Wall	Electrodes	Initial Internal
$\boldsymbol{u}^*$	$\boldsymbol{u}_{in}$	zeroGradient	noSlip	noSlip	0
p	zeroGradient	0	zeroGradient	zeroGradient	0
k^{**}	$3/2(I\,\boldsymbol{u}_{in})$	zeroGradient	0	0	Inlet
ω	Internal Field	zeroGradient	$10\frac{6\nu}{\beta_1(\Delta y_{wall})^2}$	$10\frac{6\nu}{\beta_1(\Delta y_{wall})^2}$	$10\boldsymbol{u}_{in}\,d_h^{-1}$
c	c_{in}	zeroGradient	zeroGradient	0	c_{in}

*For fully developed laminar flow analytical expressions were used both for the parallel plate and annular geometry.
**I is the turbulence intensity, varied between 5 and 20%.

Table III. Tolerance and relaxation factors.

Field	Tolerance for the linear system of eq.	Tolernace for the Residuals	Relaxaction factors
u	1×10^{-8}	1×10^{-6}	0.9
p	1×10^{-6}	1×10^{-6}	0.9
k	1×10^{-10}	1×10^{-6}	0.9
ω	1×10^{-16}	1×10^{-6}	0.9
c	1×10^{-9}	1×10^{-9}	1

analytical expressions, respectively[1,32]

$$\mathrm{Sh_y} = 1.076\left(\mathrm{ReSc}\frac{d_h}{y}\phi\right)^{1/3} \quad [16]$$

and

$$\mathrm{Sh} = 1.614\left(\mathrm{ReSc}\frac{d_h}{L}\phi\right)^{1/3} \quad [17]$$

where ϕ is 1.5 for parallel-plate electrodes, 1 for the hemicylindrical case and for a cylindrical arrangement is

$$\text{inner electrode} \qquad \phi = \frac{(1-\kappa)\left[\frac{1}{2} - \frac{\kappa^2}{1-\kappa^2}\ln\left(\kappa^{-1}\right)\right]}{\kappa\left[\frac{1+\kappa^2}{1-\kappa^2}\ln\left(\kappa^{-1}\right) - 1\right]} \quad [18]$$

$$\text{outer electrode} \qquad \phi = \frac{(\kappa-1)\left[\frac{1}{2} - \frac{\ln\left(\kappa^{-1}\right)}{1-\kappa^2}\right]}{\frac{1+\kappa^2}{1-\kappa^2}\ln\left(\kappa^{-1}\right) - 1} \quad [19]$$

being κ the ratio between the internal and external diameters. Likewise, taking into account the boundary layer theory the local and global Sherwood number for parallel-plate electrodes are given by[3,33,34]

$$\mathrm{Sh_y} = 0.335\left(\mathrm{Re}\frac{d_h}{y}\right)^{1/2}\mathrm{Sc}^{1/3} \quad [20]$$

and

$$\mathrm{Sh} = 0.664\left(\mathrm{Re}\frac{d_h}{L}\right)^{1/2}\mathrm{Sc}^{1/3} \quad [21]$$

Fig. 1 compares the local mass-transfer performance according to Eq. 16 for a parallel-plate electrochemical reactor or a cylindrical reactor with the results of the numerical calculations. In all cases an error lower than 1% between the analytical and numerical results is observed. The same comparison is made in the inset of Fig. 1 for the global mass-transfer behavior in an annular reactor showing that Eq. 17, represented as full line, coincides with the numerical calculations. Additionally, it is presented experimental results from Ross and Wragg[32,35] using the cupric sulfate system as test reaction. Taking into account the close agreement between analytical and computed results, it can be stated that the rigorous numerical solution of the fundamental equations, above declared, validates the assumptions made in the analytical procedures. Finally, the validation of the numerical calculations by comparison with analytical results must be recognized as an important preliminary step in the debugging of the proposed algorithm, that it is necessary to carry out previously the study of more complex electrochemical systems.

Developing laminar flow.—Theoretical analysis of the mass-transfer problem for an annuli without a hydrodynamic entrance length, generating a developing laminar flow, are not reported in literature. However, this case can be easily approached by means of CFD. Fig. 2 compares experimental values of the local and global Sherwood number as a function of the axial position in a parallel-plate electrochemical reactor[3] with numerical calculations represented as a full line. The local and global, given as inset, mass-transfer performance

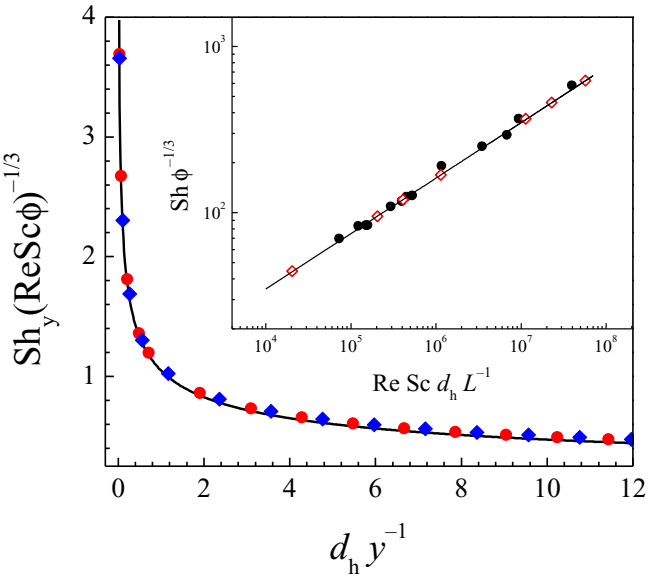

Figure 1. Local and global (inset) Sherwood number in developed laminar flow. Full lines: theoretical calculation according to Eqs. 16 and 17. (●): numerical calculation for a parallel plate. Sc = 3040, d_h = 20 mm, Re = 1315.8 and $\nu = 1.52 \times 10^{-6}$ m^2 s^{-1}. (◆): numerical calculation for an annular duct. κ = 0.5. Sc = 1000, d_h = 12.7 mm, Re = 2000 and $\nu = 1.5 \times 10^{-6}$ m^2 s^{-1}. Inset: (●): experimental results from Table I of Wragg and Ross.[35] κ = 0.5. (◇): numerical calculation with the following parameters: κ = 0.25 and 0.5, 2450 ≤ Sc ≤ 3000, 12.7 mm ≤ d_h ≤ 38.1 mm, 10 mm ≤ L ≤ 152.4 mm, 100 ≤ Re ≤ 3000 and 1×10^{-6} m^2 s^{-1} ≤ ν ≤ 1.5×10^{-6} m^2 s^{-1}.

according to Eqs. 16, 17 and 20 are also included with comparison purposes. A good agreement is detected between experimental and calculated results. Moreover, the analytical expression obtained in our previous work,[3] Eq. 22, which reproduce Eq. 20 for small y $(d_h\mathrm{Re})^{-1}$ and Eq. 16 for high y $(d_h\mathrm{Re})^{-1}$, coincides with the computed

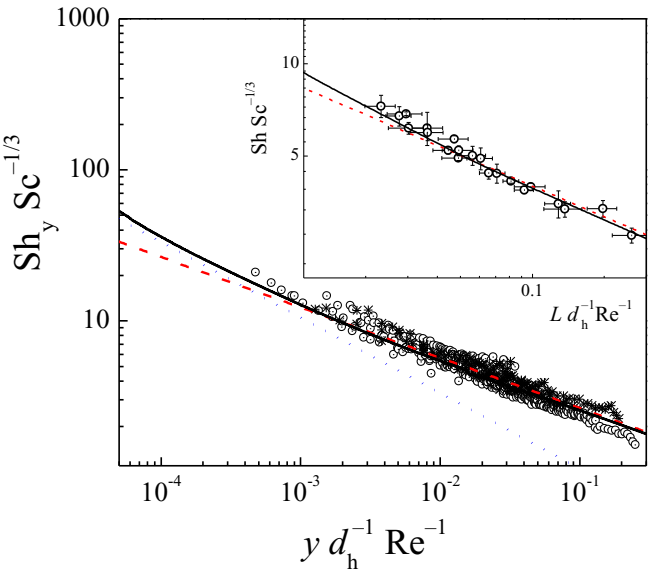

Figure 2. Local and global (inset) Sherwood number in developing laminar flow as a function of the axial position in the reactor. Experimental points: ferrycianide reduction as test reaction with electrolyte 1 (⊙) and electrolyte 2 (∗) given in Table IV. Full line: numerical calculations. Dashed line: Eq. 16 and Eq. 17 (inset) with ϕ = 1.5. Dotted line: Eq. 20. Parameters in numerical calculations: Sc = 1500, 4 mm ≤ d_h ≤ 12 mm, L = 250 mm, 100 ≤ Re ≤ 2000 and $\nu = 1.5 \times 10^{-6}$ m^2 s^{-1}.

Table IV. Properties of the electrolytes.

	Electrolyte 1	Electrolyte 2
Composition	$[K_3Fe(CN)_6] = 0.01$ M $[K_4Fe(CN)_6] = 0.01$ M $[K_2CO_3] = 0.65$ M	$[K_3Fe(CN)_6] = 0.1$ M $[K_4Fe(CN)_6] = 0.1$ M $[NaOH] = 0.5$ M
Kinematic viscosity, $m^2\ s^{-1}$	1.31×10^{-6}	8.80×10^{-7}
Diffusion coefficient, $m^2\ s^{-1}$	8.10×10^{-10}	7.50×10^{-10}
Sc	1617	1173

values.

$$Sh_y = \frac{2\frac{V_{max}}{(V_{max}-1)^{1/2}}}{3\Gamma\left(\frac{4}{3}\right)\left[\int_0^{\frac{y}{d_h Re}} \frac{V_{max}}{(V_{max}-1)^{1/2}} d\left(\frac{y}{d_h Re}\right)\right]^{1/3}} Sc^{1/3} \quad [22]$$

where V_{max} must be obtained for each $y\ (d_h Re)^{-1}$ value from the integral equation

$$\frac{y}{d_h Re} = \frac{3}{160}\int_0^{V_{max}} \frac{(V_{max}-1)(9V_{max}-7)}{V_{max}^2} dV_{max} \quad [23]$$

Fig. 3 contrasts experimental results reported by Carbin and Gabe[36] using short cylindrical electrodes with CFD calculations. It can be seen that the model reproduces the experimental results quite well for high Re Sc $d_h\ L^{-1}$, with an error lower than 10% for Re Sc $d_h\ L^{-1} > 10^5$. From Fig. 1 in the work of Carbin and Gabe[36] it seems that the experiments at low Re number are affected by natural convection, which was not taken into account in the numerical calculations. As discussed by Colli and Bisang,[3] under developing laminar flow conditions the exponent of the Reynolds number should be in the range between 1/2 and 1/3. Then, it is possible that their results at low values of Re Sc $d_h\ L^{-1}$ are distorted and show a slope similar to that given by fully developed laminar flow.

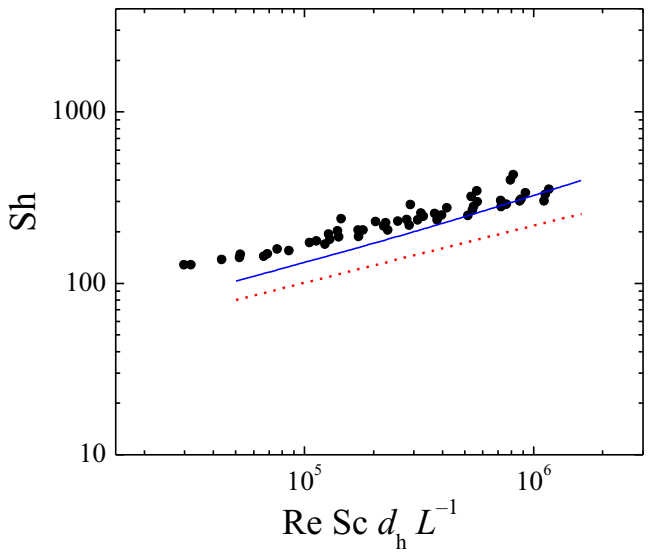

Figure 3. Global Sherwood number in developing laminar flow for a cylindrical electrochemical reactor. Full blue line: numerical calculation. (●): inner electrode in a cylindrical configuration according to Carbin and Gabe,[36] $\kappa = 0.2$. Dashed line: fully developed laminar flow, Eq. 17. Parameters in numerical calculations: Sc = 1000, $d_h = 25.38$ mm, $L = 11$ mm, $20 \le Re \le 700$ and $\nu = 1 \times 10^{-6}\ m^2\ s^{-1}$.

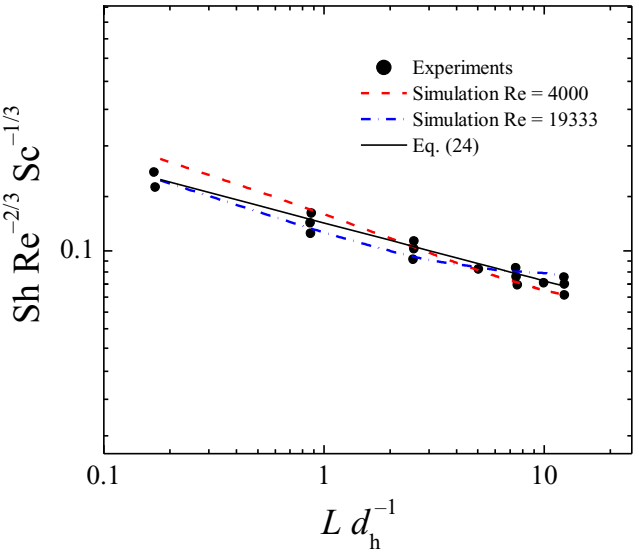

Figure 4. Global Sherwood number in the entrance region of a parallel-plate electrochemical reactor for developing mass-transfer in fully developed turbulent flow. Full line: experimental correlation, Eq. 24. Dashed and dotted lines: numerical calculation for Re = 4000 and 19333, respectively. (●): experimental values according to Pickett and Ong[9] for $Re \ge 4000$ and $L\ d_h^{-1} \le 12.5$. Parameters in numerical calculations: Sc = 2000, $d_h = 11.9$ mm, $L = 150$ mm, $4000 \le Re \le 19333$ and $\nu = 1.5 \times 10^{-6}\ m^2\ s^{-1}$.

Developing mass-transfer in fully developed turbulent flow in a parallel-plate electrochemical reactor.—Fig. 4 displays experimental results of the global Sherwood number at the inlet region of an electrochemical reactor with parallel-plate electrodes for $Re \ge 4000$ and $L\ d_h^{-1} \le 12.5$, reported by Picket and Ong,[9] which are compared with data from numerical calculations under the same conditions for Re = 4000 and 19333. Simulated results for intermediate Re numbers were found to lie between the two reported lines. Experimental results were originally correlated by Eq. 24 also showed in Fig. 4 as full line.

$$Sh = 0.125 Re^{2/3} Sc^{1/3} \left(\frac{L}{d_h}\right)^{-1/5} \quad [24]$$

Fig. 5 shows the experimental results of Pickett and Ong[9] of the global Sherwood number as a function of the Reynolds number for $L\ d_h^{-1} = 12.5$ and a comparison with numerical calculations for the same conditions. Figs. 4 and 5 reveal an excellent agreement between experimental and numerical results.

Developed mass-transfer in fully developed turbulent flow in a parallel-plate electrochemical reactor.—Fig. 6 displays calculated results, obtained by numerical differentiations of the experimental curves Sh vs. L for different L values, of the fully developed global Sherwood number as a function of the Reynolds number for an electrochemical reactor with parallel-plate electrodes, Eq. 25, reported by Pickett and Stanmore.[8] A very close agreement can be again detected between Eq. 25 and numerical results corresponding to local Sherwood numbers when they become constant at the reactor outlet.

$$Sh = 0.0278 Re^{0.875} Sc^{0.21} \quad [25]$$

It should be point out that by varying Schmidt number in the numerical calculations, we have found that Sherwood number varies with Schmidt number to the power 1/5, quite close to the correlation given by Eq. 25.

Mass-transfer in fully developed turbulent flow in a annular electrochemical reactor.—Fig. 7 compares the mass-transfer results for a concentric annulus reported by Lin et al.,[10] which were corrected taking into account diffusivity values from Saraç et al.[37] as suggested by Newman.[38] The points represent the experimental values whereas

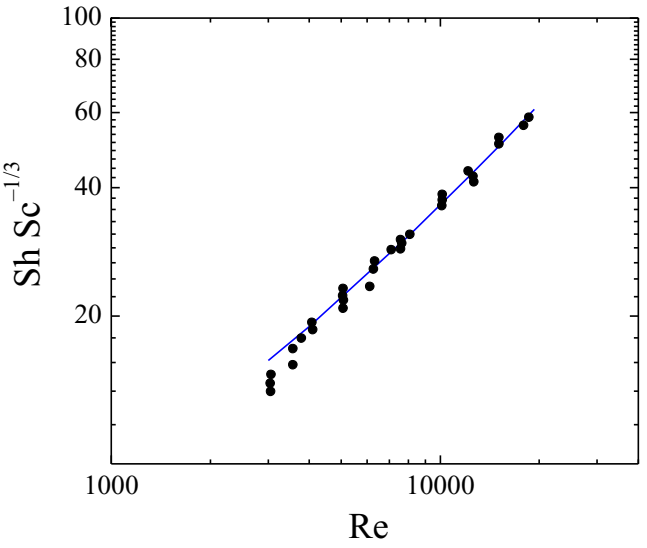

Figure 5. Relationship between global Sherwood and Reynolds numbers for developing mass-transfer in fully developed turbulent flow of a parallel-plate electrochemical reactor. Full blue line: numerical calculation. (●): experimental values, according to Picket and Ong[9] for $L\ d_h^{-1} = 12.5$. Parameters in numerical calculations: Sc = 2000, d_h = 12 mm, L = 150 mm, 3000 ≤ Re ≤ 19333 and $\nu = 1.5 \times 10^{-6}$ m^2 s^{-1}.

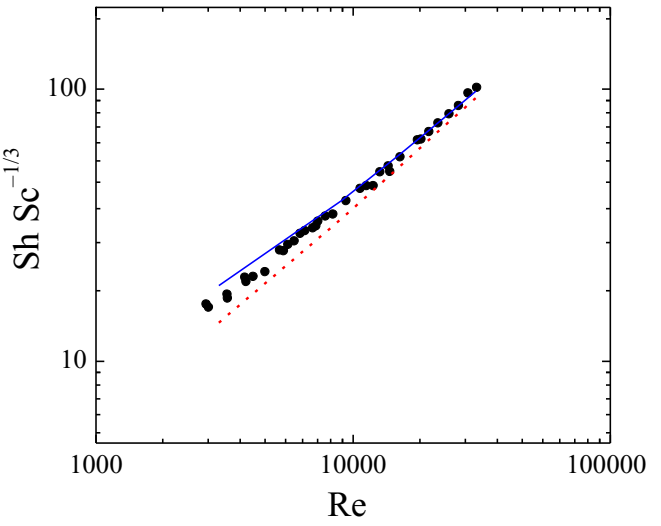

Figure 7. Global Sherwood number for an annular electrochemical reactor under fully developed turbulent flow conditions. Full blue line: numerical calculation. (●): inner electrode in a cylindrical configuration according to Lin et al.[10] which were corrected taking into account diffusivity values from Saraç et al.[37] as suggested by Newman,[38] κ = 0.5. Dashed red line: numerically obtained fully developed mass-transfer. Parameters in numerical calculations: κ = 0.5, 500 ≤ Sc ≤ 3000, d_h = 25.83 mm, L = 152.4 mm, 3000 ≤ Re ≤ 30000 and $\nu = 8.85 \times 10^{-7}$ m^2 s^{-1}.

the full line shows the numerical calculations and the dashed line reports on fully developed mass-transfer conditions, numerically obtained, corresponding to local Sherwood numbers when they become constant at the reactor outlet. The experimental and calculated results are very close being the agreement better at high values of the Reynolds number, where both lines approach to each other and also to the computed data. Despite the Sh ~ Sc$^{1/3}$ dependence showed in Fig. 7 to compare present simulations with experimental results, it should be point out that by varying Schmidt number in the numerical simulations we have found that a best representation of the experimental results can be achieved with the Schmidt number to the power 1/5.

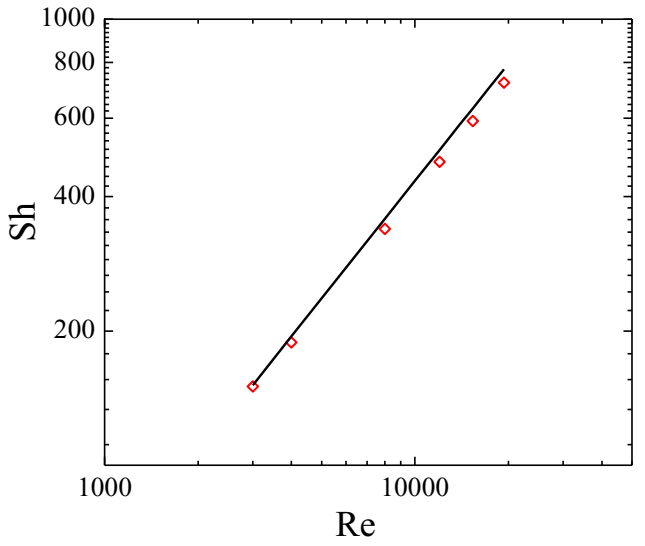

Figure 6. Global Sherwood number in fully developed mass-transfer and turbulent flow for a parallel-plate electrochemical reactor. (◇): numerical calculation. Full line: experimental correlation, Eq. 25, according to Picket and Stanmore.[8] Parameters in numerical calculations: Sc = 2000, d_h = 11.9 mm, L = 150 mm, 3000 ≤ Re ≤ 19333 and $\nu = 1.5 \times 10^{-6}$ m^2 s^{-1}.

Sudden pipe expansion.—In the equipments used in the industrial practice it is frequent a sudden expansion of the fluid at the reactor inlet producing eddies and a counterflow, which affect the mass-transfer performance. A comparison of the present turbulence model with previously reported mass-transfer measurements using a segmented electrode by Sydberg and Lotz[39] and simulation results using a low-Re k-ε turbulence model by Nešić et al.[40] for a ferri-ferrocyanide system at a sudden expansion is shown in Fig. 8. The

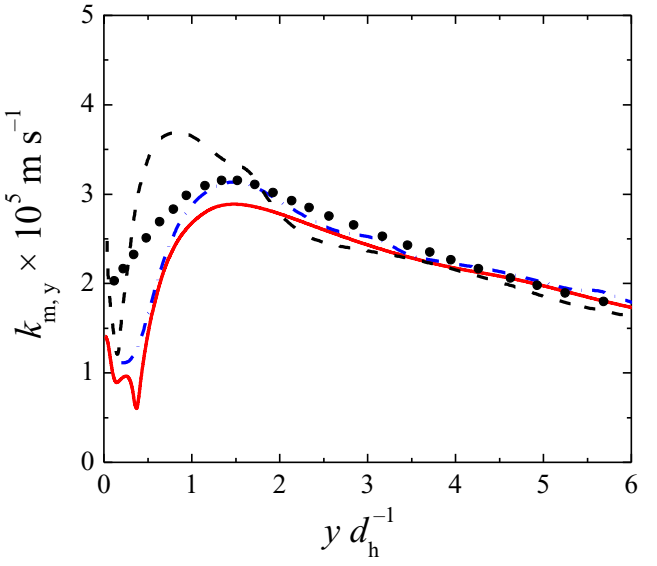

Figure 8. Local mass-transfer coefficient for a sudden pipe expansion as a function of the axial position in the reactor. (●): measurements using a segmented electrode by Sydberg and Lotz.[39] Full red line: numerical calculations without segmented electrode. Dashed dotted blue line: numerical calculations taking into account segmented electrodes and integration over each segment. Dashed black line: simulation results by Nešić et al.[40] Parameters in numerical calculations: Sc = 1460, $d_{h,in}$ = 20 mm, $d_{h,out}$ = 40 mm, L = 280 mm, Re$_{out}$ = 2.1×10^4 and $D = 6.5 \times 10^{-10}$ m^2 s^{-1}.

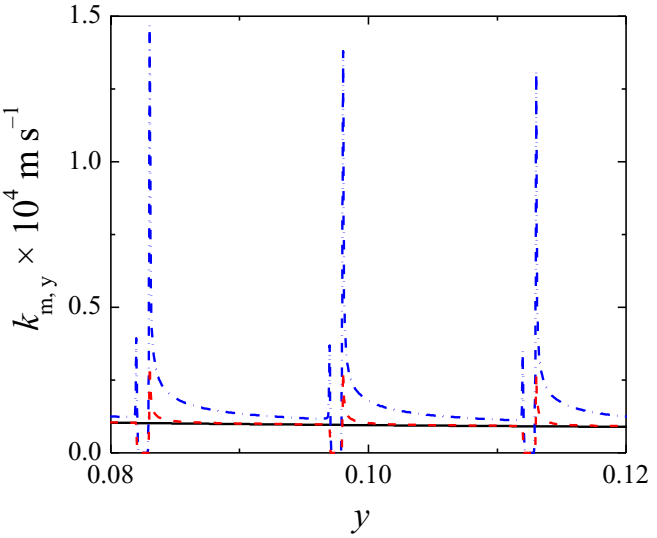

Figure 9. Influence of the insulating separator on the mass-transfer distribution. Full line: massive electrode without segments. Dashed red line: segmented electrode with level separators. Dashed dotted blue line: segmented electrode with recessed separators. Parameters in numerical calculations: 9 mm segment length, 1 mm insulation separator width, −35 μm recessed depth, Re = 6666, Sc = 3000, $D = 5 \times 10^{-10}$ m^2 s^{-1}, $d_h = 20$ mm.

data in this figure are in quite good agreement and the proposed model can accurately describe the peak position and absolute value of the local mass-transfer coefficient. The agreement is improved when the simulations are based on segmented electrodes and performing the integration of the numerically obtained current over each segment.

Segmented electrodes.—The use of a segmented electrode is a useful procedure to determine local mass-transfer coefficients. However, the insulating insertions between segments disturb the mass-transfer behavior mainly in two different ways: (i) altering the concentration profiles at the electrode surface[41] and (ii) introducing a turbulence promotion action which increases the mass-transfer conditions. To check these influences, calculations using computational fluid dynamics were performed considering three geometric configurations: (i) a segmented electrode with insulating insertions at the same level between segments, (ii) a segmented electrode with recessed insulating insertions between segments and (iii) a massive electrode without segments. The results of the modeling are reported on Figs. 9 and 10. The segments are numbered in increasing order from inlet, 1, to reactor outlet. The main geometric parameter in the calculations were 9 mm segment length, 1 mm insulation separator width, −5, −35 and −100 μm recessed depth. Fig. 9 shows that the recessed separator with a −35 μm depth has a higher influence on the mass-transfer distribution than the level case, as a consequence of the turbulence promoting action despite the small value of the recess depth. Fig. 10a) displays that when level separators are used, the enhancement factor varies within 8 and 10%, being maximum for laminar flow and

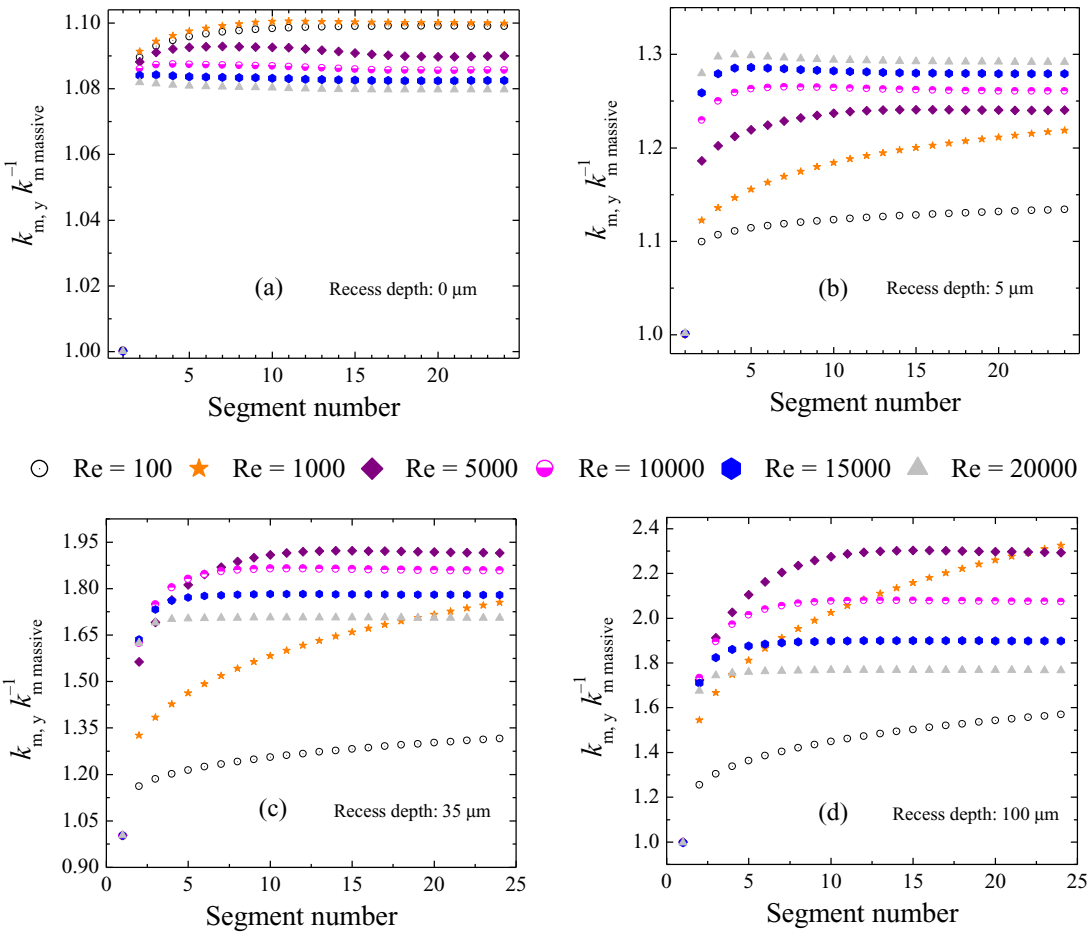

Figure 10. Influence of the insulating separators on the mass-transfer distribution for a parallel plate reactor with segmented electrodes and recessed separators in comparison to a massive electrode without segments. Parameters in numerical calculations: 9 mm segment length, 1 mm insulation separator width. Recessed depth = 0 μm, −5 μm, −35 μm and −100 μm, Re = 100, 1000, 5000, 10000, 15000 and 20000. Sc = 3000, $D = 5 \times 10^{-10}$ m^2 s^{-1}, $d_h = 10$ mm, $L = 0.25$ m.

decreasing with Re for turbulent flow. Fig. 10b) shows that for a recessed separator, −5 μm depth, the enhancement factor increases by 10–30% when Re increases being lower for laminar flow. Figs. 10c) and 10d) report that when a recessed separator with depth of −35 μm and −100 μm is used, respectively, enhancement factors vary between 15 and 130%, increasing with Re for laminar flow but decreasing with Re for turbulent flow. This strange situation can be explained accepting that enhancement factors reach a limit when the recess depth is increased; this limit depends on the hydrodynamics and it decreases faster toward lower values when Re increases. Finally, it can be observed that for laminar flow, enhancement factors increase with axial position, and for turbulent flow, enhancement factors are maximum at fully developed conditions.

There are difficulties in the application of small local electrodes to measure local mass-transfer rates caused by edge effects relating to the electrical insulation thickness. The mass-transfer enhancement increases as the local electrode size is decreased and steps between them increase in size. On the other hand, using big electrodes can cause a distortion of the local measurement due to the integration of mass-transfer coefficients in places where big slopes exist (trapezoidal rule). Thus, the proper size of a segment is a compromise between the two above opposite effects, which depends greatly on the local geometry and hydrodynamic conditions. The above analysis can explain why in the past there were found so high mass-transfer correlations when laminar and turbulent mass-transfer was measured. However, the turbulence promotion action due to the presence of small recesses at the electrode surface must be recognized as a promising and simple procedure in order to improve the performance of electrochemical reactors without high pressure drop inside the cell.[42]

Finally, with the proposed model we tried to simulate experimental results from diffusion-controlled current distributions near cell entries and corners,[43] and experimental and simulated mass-transfer in an annular duct with an obstruction.[44] Getting in both cases lower simulated mass-transfer performance than in the original works. Probably due to the presence of micro-electrodes that can add small local instabilities that increase the experimental mass-transfer behavior, as explained above.

Parallel plate electrochemical reactor with a segmented electrode.—Experiments were performed in an electrochemical reactor with a segmented cathode, 250 mm long, described elsewhere.[3] The cathode was made of 25 nickel segments, 100 mm width, 9.5 mm high and 1 mm thick. Which were insulated from one another by an epoxy resin of about 0.5 mm thick. Fig. 11 shows typical curves of the local Sherwood number as a function of the ratio between the axial position and the hydraulic diameter in the reactor. Where it can be seen that experimental points are properly represented by predictions according to the numerical simulations taking into account recessed separator with - 5 μm depth between electrodes. Since the measured mass-transfer rates are the mean values for each mass-transfer test section, the numerically predicted local Sherwood number have been averaged over each mass-transfer section. Likewise, it can be observed that a fully developed mass-transfer condition is obtained after about twelve hydraulic diameters along the electrode, as was previously concluded from experiments by Pickett and Ong.[9]

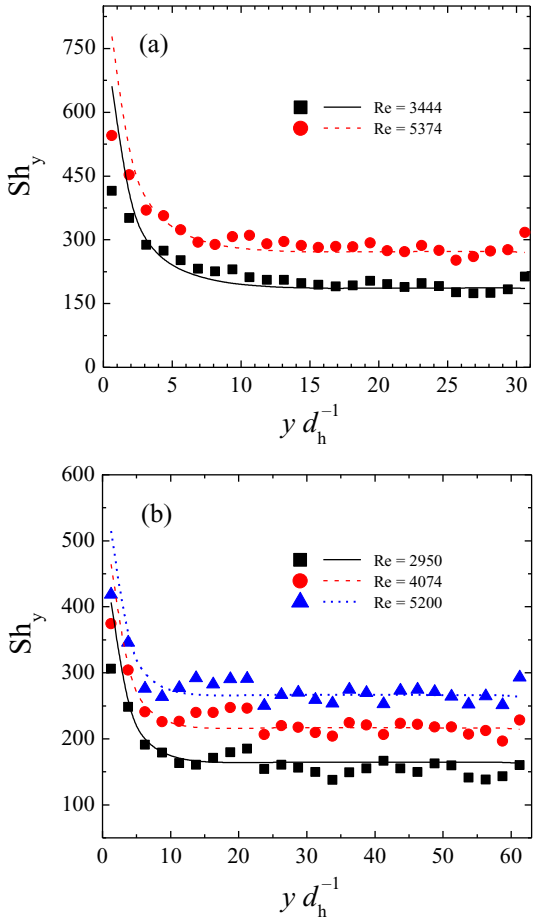

Figure 11. Local Sherwood number as a function of the ratio between the axial position and the hydraulic diameter for a segmented parallel-plate electrochemical reactor. Part (a): hydraulic diameter: 8 mm. Part (b): hydraulic diameter: 4 mm. Points: experimental results. Lines: simulated results. Experimental conditions and parameters used in numerical calculations: Electrolyte 2 given in Table IV. Properties of the reactor: 9.5 mm segment length, 0.5 mm insulation separator width. Recessed depth = −5 μm, $L = 0.25$ m.

Conclusions

It was demonstrated that CFD, when used properly, is a powerful tool to predict mass-transfer coefficients in electrochemical reactors.

The method was proved for laminar and turbulent flow, with internal recirculating velocity, and it was compared against experimental data of the authors or already reported in the literature obtaining a good agreement.

It was also found that, under turbulent flow conditions, the simplification of $Sc_T = 0.5$ can reproduce experimental results of several authors in different geometries and flow conditions.

By using segmented electrodes, higher local mass-transfer coefficient can be obtained in laminar and turbulent flows, the improvement factor will depend on the shape and amount of discontinuities between each segmented electrode and the flow conditions.

The calculation procedure corroborated that under laminar flow conditions the mass-transfer correlations depends on the Schmidt number to the usual exponent of 1/3. However, in turbulent flow an exponent around 1/5 gave a better representation of the experimental results taken into account in the present study.

The proposed calculation procedure can be recognized as a robust tool for the design of electrochemical reactors, which can be applied to diverse geometric configurations under different flow conditions. Likewise, the method can be easily coupled with potential distribution, including mass-transfer by migration and other types of kinetic control, giving an important field for forthcoming contributions.

Acknowledgments

This work was supported by the Agencia Nacional de Promoción Científica y Tecnológica (ANPCyT), Consejo Nacional de Investigaciones Científicas y Técnicas (CONICET) and Universidad Nacional del Litoral (UNL) of Argentina.

List of Symbols

a_1	constant given in Eq. 6 and Table I
c	local concentration or time-averaged concentration, mol m^{-3}
$CD_{k\omega}$	function given by Eq. 12
ct	constant given in Eq. 10
c_1	constant given in Table I and appearing in Eq. 9
$d_{o,i}$	outer, inner diameter
d_p	distance normal to the wall, m
D	diffusion coefficient, $m^2\ s^{-1}$
D_T	turbulent diffusion coefficient, $m^2\ s^{-1}$
d_h	hydraulic diameter $= 2h$, for parallel plate or $= d_o$-d_i for annulus, m
F_1	function given by Eq. 11
F_2	function given by Eq. 13
h	interelectrode gap, m
I	turbulence intensity (ratio between the root-mean-square of the turbulent velocity fluctuations and the mean velocity)
k	turbulence kinetic energy, $m^2\ s^{-2}$
k_m	mass-transfer coefficient, $m^2\ s^{-1}$
L	electrode length, m
p	density normalized pressure, $m^2\ s^{-2}$
P_k	production term given by Eq. 9, $m^2\ s^{-3}$
Re	Reynolds number $= u_{av} d_h\ \nu^{-1}$
S	invariant measure of the strain rate, s^{-1}
Sc	Schmidt number $= \nu\ D^{-1}$
Sc_T	turbulent Schmidt number $= \nu_T\ D_T^{-1}$
Sh	Sherwood number defined in Eqs. 1 or 2
$\boldsymbol{u}$	local fluid velocity or time-averaged fluid velocity, $m\ s^{-1}$
V_{max}	implicit function given by Eq. 23
y	axial coordinate, m
z	axial coordinate, m
∇	Nabla operator

Greek

α	constant given in Table I and appearing in Eq. 8
β	constant given in Table I and appearing in Eq. 8
β^*	constant given in Table I and appearing in Eqs. 7, 11, 13 and 9
Γ	gamma function
Δy_{wall}	distance to the next computational point away from the wall
ε	turbulence dissipation, $m^2\ s^{-3}$
κ	annulus ratio $= d_i\ d_o^{-1}$
ν	kinematic viscosity, $m^2\ s^{-1}$
ν_T	turbulent kinematic viscosity, $m^2\ s^{-1}$
σ_k	constant given in Table I and appearing in Eq. 7
σ_ω	constant given in Table I and appearing in Eq. 8, 11 and 12
ϕ	function dependent of the geometry and κ
ω	turbulence frequency or specific dissipation rate, s^{-1}

Subscripts

av	average value
b	bulk
i	inner
in	inlet
o	outer
out	outlet
y	the variable is referred to the y coordinate
z	the variable is referred to the z coordinate
1	inner constant given by the k-ω model
2	outer constant given by the k-ε model

ORCID

A. N. Colli https://orcid.org/0000-0002-0983-1842

References

1. D. J. Pickett, *Electrochemical Reactor Design*, Elsevier, Amsterdam (1979).
2. A. N. Colli and J. M. Bisang, *J. Electrochem. Soc.*, **164**, E42 (2017).
3. A. N. Colli and J. M. Bisang, *J. Electrochem. Soc.*, **160**, E5 (2013).
4. F. P. Berger and K. F. F. L. Hau, *Int. J. Heat Mass Transfer*, **20**, 1185 (1977).
5. P. V. Shaw, L. P. Reiss, and T. J. Hanratty, *AlChE J*, **9**, 362 (1963).
6. S. Aravinth, *Int. J. Heat Mass Transfer*, **43**, 1399 (2000).
7. D. W. Hubbard and E. N. Lightfoot, *Industrial & Engineering Chemistry Fundamentals*, **5**, 370 (1966).
8. D. J. Pickett and B. R. Stanmore, *J. Appl. Electrochem.*, **2**, 151 (1972).
9. D. J. Pickett and K. L. Ong, *Electrochim. Acta*, **19**, 875 (1974).
10. C. S. Lin, E. B. Denton, H. S. Gaskill, and G. L. Putnam, *Industrial & Engineering Chemistry*, **43**, 2136 (1951).
11. F. M. White, *Fluid Mechanics*, McGraw-Hill (2003).
12. J. O. C. Jones, *J. Fluids Eng.*, **98**, 173 (1976).
13. J. O. C. Jones and J. C. M. Leung, *J. Fluids Eng.*, **103**, 615 (1981).
14. Y. Wang, J. Postlethwaite, and D. J. Bergstrom, *J. Appl. Electrochem.*, **26**, 471 (1996).
15. D. C. Wilcox, *Turbulence Modeling for CFD*, DCW Industries (2006).
16. M. Rosales and J. L. Nava, *J. Electrochem. Soc.*, **164**, E3345 (2017).
17. E. P. Rivero, M. R. Cruz-Díaz, F. J. Almazán-Ruiz, and I. González, *Chem. Eng. Res. Des.*, **100**, 422 (2015).
18. W. Rodi and G. Scheuerer, *J. Fluids Eng.*, **108**, 174 (1986).
19. F. R. Menter, *AIAA Journal*, **32**, 1598 (1994).
20. J. E. Bardina, *Turbulence Modeling Validation, Testing, and Development*, National Aeronautics and Space Administration, Ames Research Center (1997).
21. F. R. Menter, *International Journal of Computational Fluid Dynamics*, **23**, 305 (2009).
22. C. Rosén and C. Trägårdh, *The Chemical Engineering Journal and the Biochemical Engineering Journal*, **59**, 153 (1995).
23. G. Nelissen, B. Van Den Bossche, J. Deconinck, A. Van Theemsche, and C. Dan, *J. Appl. Electrochem.*, **33**, 863 (2003).
24. B. Lin and K. Shiono, *Journal of Hydraulic Research*, **33**, 773 (1995).
25. Y. Tominaga and T. Stathopoulos, *Atmos. Environ.*, **41**, 8091 (2007).
26. C. Gualtieri, A. Angeloudis, F. Bombardelli, S. Jha, and T. Stoesser, *Fluids*, **2**, 17 (2017).
27. H. G. Weller, G. Tabor, H. Jasak, and C. Fureby, *Computers in Physics*, **12**, 620 (1998).
28. H. H. K. Versteeg and W. Malalasekera, *An Introduction to Computational Fluid Dynamics: The Finite Volume ,Method*, Pearson Education Limited, (2007).
29. J. H. Ferziger and M. Perić, *Computational Methods for Fluid Dynamics*, Springer London, Limited, (2002).
30. A. N. Colli, (2018), https://github.com/ancolli/concLaminarTurbulentFoam.
31. R. B. Bird, W. E. Stewart, and E. N. Lightfoot, *Transport Phenomena*, 2nd edition, John Wiley & Son, New York (2002).
32. T. K. Ross and A. A. Wragg, *Electrochim. Acta*, **10**, 1093 (1965).
33. E. R. G. Eckert and R. M. Drake, *Heat and mass transfer, 2nd edition*, p. 530, McGraw-Hill, New york, (1985).
34. V. Levich, *Physicochemical Hydrodynamics*, p. 700, Prentice Hall, New Jersey, (1962).
35. A. A. Wragg and T. K. Ross, *Electrochim. Acta*, **13**, 2192 (1968).
36. D. C. Carbin and D. R. Gabe, *Electrochim. Acta*, **19**, 653 (1974).
37. H. Saraç, M. A. Patrick, and A. A. Wragg, *J. Appl. Electrochem.*, **23**, 51 (1993).
38. J. Newman and K. E. Thomas-Alyea, *Electrochemical Systems, 3rd edition*, Wiley-Interscience (2004).
39. T. Sydberger and U. Lotz, *J. Electrochem. Soc.*, **129**, 276 (1982).
40. S. Neŝić, G. Adamopoulos, J. Postlethwaite, and D. J. Bergstrom, *The Canadian Journal of Chemical Engineering*, **71**, 28 (1993).
41. O. Wein and K. Wichterle, *Collect. Czech. Chem. Commun.*, **54**, 3198 (1989).
42. A. N. Colli, R. Toelzer, M. E. H. Bergmann, and J. M. Bisang, *Electrochim. Acta*, **100**, 78 (2013).
43. A. A. Wragg, D. J. Tagg, and M. A. Patrick, *J. Appl. Electrochem.*, **10**, 43 (1980).
44. G. Weyns, G. Nelissen, J. G. A. Pembery, P. Maciel, J. Deconinck, H. Deconinck, M. A. Patrick, and A. A. Wragg, *J. Appl. Electrochem.*, **39**, 2453 (2009).